Tarach, K.; Gora-Marek, K.; Tekla, J.; Brylewska, K.; Datka, J.; Mlekodaj, K.; Makowski, W.... (2014). Catalytic cracking performance of alkaline-treated zeolite Beta in the terms of acid sites properties and their accessibility. Journal of Catalysis. 312:46-57. doi:10.1016/j.jcat.2014.01.009.

# CATALYTIC CRACKING PERFORMANCE OF ALKALINE TREATED ZEOLITE BETA IN THE TERMS OF ACID SITES PROPERTIES AND THEIR ACCESSIBILITY

K. Tarach[a], K. Góra-Marek[a*], J. Tekla[a], K. Brylewska[a], J. Datka[a], K. Mlekodaj[a], W. Makowski[a], M.C. Igualada López [b], J. Martínez Triguero[b], F. Rey[b]

[a] *Faculty of Chemistry, Jagiellonian University in Kraków, Ingardena 3, 30-060 Kraków, Poland*

[b]*Instituto de Tecnología Química, Universidad Politécnica de Valencia, Camino de Vera s.n., 46022 Valencia, Spain*

*corresponding author: kinga.goramarek@gmail.com*

*phone:+48 12 663 20 81*

## ABSTRACT

The zeolite Beta is considered as a promising additive for FCC catalyst in diesel oil production. In this article, it is shown that hierarchical zeolite Beta obtained by an optimized desilication procedure increases Diesel and propylene yields during gas-oil cracking reaction. The alkaline treatment of zeolite Beta (Si/Al = 22) by desilication with NaOH and NaOH&TBAOH was investigated. The catalytic performance improvement of desilicated zeolite Beta has been rationalized by deep characterization of the samples including X-ray diffraction, low temperature adsorption of nitrogen, solid-state $^{29}$Si MAS NMR and IR studies of acidity. Finally, the catalytic performance of the zeolites Beta was evaluated in the cracking of *n*-decane, 1,3,5-tri-iso-propylbenzene and vacuum gas oil. It was found that desilication with NaOH&TBAOH ensures the more uniform intracrystalline mesoporosity with the formation of narrower mesopores, while preserving full crystallinity resulting in catalysts with the most appropriated acidity and then, with better catalytic performance.

*Keywords*

hierarchical zeolites, Beta, desilication, acidity, TIPB, *n*-decane, cracking, FCC

## 1. INTRODUCTION

Zeolites are well known catalysts of high surface area, high hydrothermal and thermal stability, structural pores of molecular dimensions, and hosting strong Brønsted and Lewis acid sites. These unique properties are responsible for their application as catalysts in many major chemical processes [1, 2]. The main advantages of the micropores of molecular dimensions are their extremely high surface area and shape selectivity. However, also diffusional limitations are frequently observed when large molecules are processed, which induce fast catalyst deactivation [3]. To improve the catalyst effectiveness in chemical reactions, desilication i.e. controlled silicon extraction from the zeolite framework in alkaline aqueous solution has been developed as one of the most efficient methods to design micro- and mesoporous (hierarchical) zeolites [4, 5]. The desired intracrystalline mesoporosity is ruled by the interplay of micro- and mesopores and is, however, influenced by the value of the framework Si/Al ratio [6, 7]. It has been reported that aluminium atoms in framework positions play a crucial role in silicon extraction directing the mesopore formation process, as the $AlO_4^-$ tetrahedra are reported to protect Si atoms in the neighbourhood against $OH^-$ ions attack due to electrical repulsion [8]. Alkaline leaching, performed in aqueous NaOH and tetraalkylammonium hydroxides mixtures, leads to the dissolution of both Si and smaller amounts of Al species from the framework. Nevertheless, most of these extracted Al species are able to realuminate on the mesopore surface, resulting in the lowering the Si/Al ratio of the hierarchical [9, 10]. Zeolite desilication has been successfully applied to produce a large number of hierarchically structured zeolites MFI [11, 12]MTW [13], MOR[14, 15], FER [16, 17], FAU [18], and Beta [19, 20]. Nevertheless, the benefits of desilicated zeolite Beta for catalytic cracking reaction have not been shown in previous studies.

Zeolite Beta belongs to a complex family, consisting in intergrowth of two polymorphs (polymorph A and B) [21, 22] and it is characterized by a 3D channel system formed by micropores limited by 12-MR windows (ca. 0.7 nm in diameter). The remarkably lower stability of zeolite Beta structure during desilication in comparison to ZSM-5 and mordenite has been reported [20]. Also, the influence of framework aluminum content for controlled desilication was shown [8]. Therefore, it can be assumed that the low stability of Al atoms in the framework positions in zeolite Beta [23], caused by the presence of high concentration of structural defects [24], can also affect the desilication process and the high amount of EFAL species can be detected. Framework silicon extraction from zeolite Beta (Si/Al = 220) upon treatment with NaOH revealed the extensive mesopore formation of

intracrystalline nature, meanwhile the micropore volume and crystallinity of the desilicated materials was severely reduced [19]. This clearly show that basic treatments, even at mild conditions, destructively affect the structural and acidic properties of zeolite Beta, contrarily to that observed on MFI, MOR and MTW [11, 12].

The application of desilicated hierarchical large pore zeolites for gasoil cracking have been recently studied for zeolite USY [25] and mordenite [26].In these studies the mesoporosity enhancement increases the yield of middle distillates, while preserving or even increasing overall catalytic activity and olefinicity in $C_3$-$C_4$ gas fraction. Zeolite Beta has been considered as an alternative to ZSM-5 as potential additive for the USY-based FCC catalyst for increasing $C_3$-$C_4$ olefins with low penalty in the yield of gasoline [27, 28, 29].However, the commercial use of zeolite Beta as FCC additive is limited due to its faster deactivation when compared to ZSM-5.

In this work, we describe first study of the applicability of hierarchical zeolite Beta for industrially relevant gas oil cracking reaction. The catalytic performance, including gas oil, *n*-decane and TIPB cracking on hierarchical zeolites Beta has been explained on the basis of their textural and acidic properties. We demonstrate that an optimized desilication procedure able to produce well controlled mesoporosity in zeolite Beta improves the catalytic performance, increasing its overall gas-oil cracking activity with high yields to propylene and middle distillates and lower coke production.

## 2. EXPERIMENTAL

### 2.1. Catalyst preparation

The parent zeolite $NH_4$Beta of Si/Al = 22 was purchased from Zeolyst (CP814C). Desilication was carried out in the 0.2 M solutions of NaOH and NaOH&TBAOH (tetrabutylammonium hydroxide) mixture (TBAOH/(NaOH+TBAOH) = 0.4) at the temperature of 65 $^oC$ for 0.5 h. After desilication the suspension was cooled down in ice-bath, filtered and washed with distillate water until neutral pH. Next fourfold $Na^+/NH_4^+$ ion-exchange with 0.5 M $NH_4NO_3$ was performed at 60 $^oC$ for 1 h. Finally, the resulting samples were again filtrated, washed and dried at room temperature.

### 2.2. Characterization methods

The powder X-ray diffraction (XRD) measurements were carried out using a PANalytical Cubix X'Pert Pro diffractometer, with $CuK_\alpha$ radiation, $\lambda$=1.5418 Å in the 2$\theta$ angle range of 2-40°. Powder X-ray patterns were used for structural identification of the relative crystallinity value (%Cryst) for all the zeolites. The determination of the relative crystallinity value was based on the intensity of the characteristic peaks in the range between 20.0$^o$ to 24.0$^o$.

Si and Al content in the parent and desilicated zeolites were determined by ICP OES spectroscopy on an Optima 2100DV (PerkinElmer) instrument.

The X-ray photoelectron spectra (XPS) were measured on a Prevac photoelectron spectrometer equipped with a hemispherical VG SCIENTA R3000 analyser. The photoelectron spectra were measured using a monochromatized aluminum $AlK_\alpha$ source (E=1486.6 eV) and a low energy electron flood gun (FS40A-PS) to compensate the charge on the surface of nonconductive samples. The base pressure in the analysis chamber during the measurements was $5 \cdot 10^{-9}$ mbar. Spectra were recorded with constant pass energy of 100 eV for the survey and for high resolution spectra. The binding energies were referenced to the Si 2p core level (103.0 eV). The composition and chemical surrounding of the sample surface were investigated on the basis of the areas and binding energies of Al 2p, Si 2p and O 1s photoelectron peaks. The fitting of high resolution spectra was provided through the CasaXPS software.

The solid state MAS NMR spectra were acquired on an APOLLO console (Tecmag) at the magnetic field of 7.05 T (Magnex). For the $^{29}Si$ MAS-NMR spectra a 3 μs rf pulse (π/2 flipping angle) was used, 4 kHz spinning speed, and 256 scans with the delay of 40 s were acquired. The $^{27}Al$ spectra were recorded using the 2 μsrf pulse (π/6 flipping angle), 8 kHz spinning speed, and 1000 scans with acquisition delay 1 s. The frequency scales in ppm were referenced to TMS and to 1 M solution of $Al(NO_3)_3$, for the $^{29}Si$ and $^{27}Al$ spectra, respectively. The spectra were normalized to the mass of sample.

The $N_2$ sorption processes at -196 $^oC$ were studied on an ASAP 2420 Micromeritics after activation in vacuum at 400 $^oC$ for 12 h. Surface Area ($S_{BET}$) and micropore volume ($V_{micro}$) were determined by applying the BET and *t*-plot methods, respectively. Pore size distribution and volume of mesopores ($V_{meso}$) were obtained by applying the BJH model to the adsorption branch of the isotherm.

The QE-TPDA measurements of *n*-hexane and *n*-nonane were performed with use of the flow TPD system equipped with thermal conductivity detector (Micro Volume TCD, Valco) presented more into detail earlier [30, 31]. Prior each measurement a sample (ca. 10 mg) was activated by heating in He flow (10 °C/min to 500°C). Adsorption was carried out at room temperature by replacing pure helium used as the carrier gas with helium containing small concentration of hydrocarbon (ca 0.4 vol%). After completed adsorption the QE-TPDA experiment was performed by cyclic heating and cooling the sample (2 or 10 °C/min up to 500 °C) in He/HC flow (6.5 $cm^3$/min). Desorption-adsorption cycles were separated with 1 h isothermal segments at room temperature. In the micro- and mesopore volume calculations, the experimental desorption maxima were integrated and related to the calibration data. Density of the adsorptive was assumed as equal to that of the liquid.

For FTIR studies, the samples were pressed into the form of self-supporting discs (ca. 5 mg/$cm^2$) and evacuated in a quartz IR cell at 530 $^oC$ under vacuum for 1 h. Spectra were recorded with a Bruker Equinox 55 spectrometer equipped with a MCT detector. The spectral resolution was of 2 $cm^{-1}$. The CO adsorption was performed at -100 $^oC$. Pyridine (Py) was adsorbed at 170 $^oC$, the concentration of Brønsted and Lewis acid sites determined in quantitative IR studies of pyridine adsorption, according to the procedure given in ref. [32]. The values of 0.10 $cm^2$/μmol and 0.07 $cm^2$/μmol were obtained for the 1450 $cm^{-1}$ band of pyridine coordinatively bonded to Lewis sites (PyL) and for the 1545 $cm^{-1}$ band of pyridinium ion ($PyH^+$), respectively. The ammonia adsorption experiments were performed according to

following procedure. An excess of ammonia, sufficient to neutralize all the acid sites, was adsorbed at 130 ºC [33] and the physisorbed molecules were removed by evacuation at the same temperature. The concentration of Brønsted and Lewis sites was calculated from the intensities of 1450 $cm^{-1}$ and 1620 $cm^{-1}$ bands of ammonium ions ($NH_4^+$) and ammonia interacting with Lewis sites ($NH_3L$) and their extinction coefficients. The extinction coefficient of $NH_4^+$ 1450 $cm^{-1}$ band was determined as a slope of the linear dependence of the intensity of this band versus the amount of ammonia adsorbed in zeolite NaHY containing only protonic sites (the value 0.11 $cm^2/\mu mol$ was obtained). The extinction coefficient of $NH_3L$ band was determined in the experiments in which ammonia was sorbed in zeolite HY dehydroxylated at 800 ºC containing practically only Lewis acid sites. The value of extinction coefficient was calculated from the linear dependence of 1620 $cm^{-1}$ band versus the amount of ammonia interacting with Lewis sites (the amount of ammonia sorbed minus the amount of ammonia reacting with protonic sites, the small amount of which remained upon pre-treatment at 1070 K). The value 0.026 $cm^2/\mu mol$ was obtained.

### 2.3. Catalytic cracking tests

The cracking experiments were performed in a MAT (Micro Activity Test) unit described previously [34, 35]. Pellets of zeolites were crushed and sieved; fraction of the 0.59–0.84 mm was taken for cracking reactions. For each catalyst, catalytic experiments were carried out, preserving the amount of catalyst (cat) constant and varying feeds amounts (oil). Three cracking reactions with different cat-to-oil ratios of 1,3,5-tri-iso-propylbenzene (TIPB) were performed at 500 ºC and for 60 s time on stream (TOS), with 200 mg of catalyst. For *n*-decane cracking at 500 ºC and for 60 s TOS,300 mg of catalyst was diluted in 2.5 g of inert silica, and five experiments were performed. In case of gas oil cracking five experiments with different cat-to-oil ratio were also performed and 500 mg of catalyst was diluted in 2.5 g of inert silica; with reaction temperature of 520 ºC and with TOS of 30 s. For first and last experiments the amount of feed was maintained in order to investigate the stability of catalysts. Gases were analysed by Gas Chromathography in a Rapid Refinery Gas Analyser from Bruker (450-GC) and simulated distillation of liquids in a Bruker SIMDIS. LCO was analysed by comprehensive two-dimensional gas chromatography (GC × GC) on a Agilent 7890A GC described elsewhere[36].

Kinetic rate constants (K) were calculated by fitting the conversions (X) to a first-order kinetic equation for a plug flow reactor (1) for *n*-decane and TIPB or to a second order

kinetic equation for a plug flow reactor (2) for gas oil, assuming that the deactivation is enclosed in the kinetic constant and taking into account the volumetric expansion factor (3),

$$K = -(\text{cat oil}^{-1}\text{TOS})^{-1}[\varepsilon X + (1+\varepsilon)\ln(1-X)] \quad (1)$$

$$K = -(\text{cat oil}^{-1}\text{TOS})^{-1}[X/(1-X)] \quad (2)$$

$$\varepsilon = (\Sigma\text{molar selectivities of products}) - 1 \quad (3)$$

These rate constants were used to compare the activities of the catalysts with their textural and acidic properties.

# 3. RESULTS AND DISCUSSION

## 3.1. Structural and chemical analysis of hierarchical zeolites Beta

### *3.1.1. XRD results*

The XRD patterns (Figure 1) of parent and desilicated zeolites present the typical diffraction pattern of zeolite Beta. The % of crystallinity of desilicated samples is given in Table 1. It can be noticed that desilication with NaOH&TBAOH mixture did not decrease the crystallinity of resulting material. On the contrary, there is an important loss of crystallinity for NaOH treated samples, resulting in a relative drop of crystallinity down to 66%, what indicates that the desilication with pure NaOH leads to partial amorphisation of Beta zeolite as has been observed previously [19, 20]. Low stability of Beta zeolite under NaOH treatment is in a line with previous studies [19] that reported complete amorphisation upon NaOH treatments.

The influence of aluminium content on desilication processes and stability of zeolite structure under alkaline treatment have been widely discussed in literature [8]. It is generally accepted that $AlO_4^-$ tetrahedra are protect neighbouring Si atoms against the $OH^-$ attack. Therefore zeolites of low Si/Al are less prone to both Si extraction and to amorphisation. According to the data presented in Figure 1, the addition of TBAOH to the desilication media protects zeolite against amorphisation, pointing to the important role of TBAOH in this process. Similar results were reported by Verboekend et al. [19], who studied the effect of the addition of various organic cations to NaOH on porosity and structure of zeolites Beta and USY.

### *3.1.2. Bulk and Surface chemical compositions: Chemical analyses and XPS.*

Selective silicon extraction during alkaline treatment results in the decrease of Si/Al ratio of obtained hierarchical Beta zeolites, from 22 to 13 and 16 (Table 1), for zeolites treated with NaOH and with NaOH&TBAOH solutions, respectively. Less extensive desilication of zeolite Beta in presence of TBAOH is assigned to its protective influence on zeolite structure, resulting from the known affinity of quaternary organic cations to surface of zeolites [37, 38]. The analysis of filtrate solutions obtained after desilication confirmed high selectivity of alkaline treatments for silicon extraction, and as expected higher amount of Si was extracted during NaOH treatment. Additionally, this silicon extraction was accompanied by minor aluminum removal (Table 1).

One of the most important features responsible for enhanced catalytic performance in hierarchical zeolites is presence of aluminium gradients across the zeolite crystals. To answer the question XPS measurements were performed. Table 1 shows $(Si/Al)_{bulk}$ from chemical analysis and $(Si/Al)_{surf}$ from XPS experiments. The $(Si/Al)_{surf}/(Si/Al)_{bulk}$ ratio informing on Si or Al excess or deficit on grain surface if comparing with the bulk are presented as well. The $(Si/Al)_{surf}/(Si/Al)_{bulk}$ of parent zeolite is higher than 1 indicating that the external surface of parent material is enriched in silicon respect to the bulk, while in alkaline treated solids the reverse situation occurs (i.e. their external surfaces are enriched in Al). This can be rationalized by considering that the chemical attack of hydroxyl anions will occur preferentially at the external surface of the solids and therefore, selective Si extraction will occur at the outer part of the zeolite particle. Now, comparing the external Al concentration of NaOH treated sample to that obtained upon NaOH&TBAOH desilication, it is observed that the Al enrichment of former sample is more pronounced than in the latter material. This is an evidence of the protective role of $TBA^+$ cations during desilication. They are attached at the external surface of the Beta zeolite, since has strong diffusional limitations, and force NaOH to enter pores and then attack the zeolite from inside the structure [39, 40]. This resulted in more homogeneous desilication across the zeolite particle, being the external and bulk Si/Al ratios very similar (Table 1).

It is generally accepted that neighbouring Al atoms in negatively charged tetrahedra $AlO_4^-$ are responsible for the protection of Si atoms against $OH^-$ attack. As result, the enriched in $AlO_4^-$ surface zone of highly siliceous zeolite ZSM-5 is more resistant for desilication in basic solutions than the bulk of crystal [32, 41]. In zeolite Beta surface zone is poorer in Al than the bulk; therefore the Si atoms extraction is more effective form the surface zone than from the bulk.

### *3.1.3. The $^{29}$Si MAS NMR results*

The $^{29}$Si MAS NMR spectra (normalized to the sample mass) of parent zeolite and desilicated zeolites are presented in Figure 2. The spectrum of the parent zeolite shows an strong signal at 112 ppm of Si(4Si,0Al) and a less intense one at 105 ppm assigned to Si(3Si,1Al) unit. The desilication with 0.2 M NaOH and NaOH&TBAOH results in a decrease of the intensity of the Si(4Si,0Al) signal due to decrease of the Si/Al ratio of the sample upon desilication. It is noteworthy to notice that the Si(3Si,1Al) signal practically does not change upon desilication. All these findings indicate that Si atoms bonded (*via* oxygens)

to four Si in Si(4Si,0Al) units are extracted by the alkaline treatment in the first order and before those Si atoms which are placed in the neighbourhood of the Si(3Si,1Al) units. In other words, the presence of $AlO_4^-$ stabilizes neighbouring Si atom (in the Si(OH)Al groups) by the repulsion of $OH^-$ ions. Similar results were reported in our earlier study on the desilication of zeolite ZSM-5 [41].

### 3.2. Textural properties of desilicated zeolites Beta

#### *3.2.1. Low temperature $N_2$ adsorption studies*

The isotherms measured for the parent zeolite Beta can be identified as the type I typical of purely microporous material (Figure 3). The analysis of low temperature $N_2$ adsorption isotherm of the parent zeolite (Table 2) shows the presence of minor mesopore surface area and large micropore volume (0.18 $cm^3g^{-1}$) as typically found for zeolite Beta.

The treatment of the parent zeolite Beta with alkaline solution resulted in larger uptake of $N_2$ at high relative pressures in the isotherms (Figure 3). This is a clear indication of higher adsorption capacity in the mesopore range of the desilicated samples in comparison to the parent zeolite. Indeed, the adsorption isotherms for desilicated samples are typical of materials containing both micro and mesoporosity and can be classified as type IV isotherms. The analysis of the corresponding isotherms show that the micropore volume of NaOH treated zeolite decreases, being consistent with the XRD results and evidences the loss of crystallinity for NaOH desilicated zeolite with respect to the parent material. However, the analysis if the $N_2$ adsorption isotherm of zeolite treated with NaOH&TBAOH shows that most of the microporosity is preserved upon alkaline treatment in good agreement to XRD results. This clearly indicates that NaOH&TBAOH treatment for desilication of zeolite Beta has a less aggressive effect on the zeolite structure.

Also, the TEM micrographs (Figure 4) indicate that, at macroscopic level, the desilication mechanism of NaOH&TBAOH is different than that in NaOH media. In Figure 4c, it is seen that samples treated with NaOH&TBAOH shows a more uniform mesopore system that spreads through the whole zeolite particle, while the NaOH treatment results in a core-shell particle (Figure 4b) in which mesoporosity is located at the external surface of the particle and the inner part remains almost unmodified.

In addition, the influence of TBAOH as pore directing agent can be obtained from BJH pore size distribution analysis of the $N_2$ adsorption isotherms pointing to the formation of

mesopores of narrower average diameter in comparison to pure NaOH treatment (Fig. 3). Finally, it can be concluded that the desilication performed in the presence of TBAOH results in the formation of a mesoporous secondary system, while preserving the crystallinity of the zeolite Beta.

### *3.2.2. The QE-TPD results of alkanes adsorption*

The QE-TPDA profiles of *n*-hexane, shown in Figure 5a, exhibit a similar high temperature maximum at 180 °C, resulting from desorption of the molecules filling the micropores. Similar thermodesorption profiles were already reported for Beta zeolites [31]. Additional low temperature desorption maxima at 35 °C, observed for the desilicated zeolites should be attributed to the strong adsorption sites on the mesopore surface [42]. Values of the pore volume calculated by integration of the QE-TPDA profiles, are compared in Table 2 with the corresponding values obtained from $N_2$ adsorption data. For the desilicated zeolites corrected values of the micropore volume, with contributions of the low temperature peaks subtracted, are also shown. Both QE-TPDA profiles and adsorption capacity data show that desilication with NaOH resulted in considerable decrease of the micropore volume, while for NaOH&TBAOH desilicated zeolite it remained unchanged. This may indicate that in case of zeolite Beta treated with pure NaOH some part of the dissolved zeolitic matrix formed amorphous aluminosilicates.

The QE-TPDA profiles of *n*-nonane, plotted in Figure 5b, were recorded in temperatures limited to 120 °C, in order to eliminate negative effects of catalytic reactions of *n*-nonane (observed above 300 °C) on porosity of the studied samples. Based on these QE-TPDA profiles, the pore size distributions (Figure 5c) were calculated according to the modified BJH scheme [43]. These results show that desilication with NaOH results in formation of larger and wider pores, while use of NaOH&TBAOH as a desilicating agent leads to formation of narrower and more uniform mesopores. These results fully agree to that concluded from $N_2$ isotherms and TEM studies as discussed above.

## 3.3. Acid properties of zeolites

### *3.3.1. The Si(OH)Al groups*

The spectra of the hydroxyls groups in parent and desilicated zeolites are presented in Figure 6. The 3604-3714 $cm^{-1}$ band of the acidic Si(OH)Al groups, the 3730 $cm^{-1}$ band of the Si-OH in defects and the 3740 $cm^{-1}$ of silanols on external surfaces and mesopore surfaces can

be distinguished. The desilication of Beta zeolite, both with NaOH and NaOH&TBAOH mixture, led to the distinct increase of the silanols amount on mesopore surfaces. This enhancement is particularly significant for zeolite treated with NaOH and corresponds to the development of mesoporosity (Table 2). The slight increase of the acidic hydroxyls band is related to the increase of Al content in zeolite framework. The maximum shift of the Si(OH)Al band to higher frequency points toward decrease of acid strength after desilication. The acid strength of desilicated zeolites will be deeper discussed when considering the results of CO and pyridine adsorption studies (Section 3.3.4).

### *3.3.2. The concentration of Brønsted and Lewis acid sites*

The concentration of both Brønsted and Lewis acid sites was determined by quantitative IR studies of pyridine (Py) and ammonia ($NH_3$) adsorption experiments.

The values of the concentrations of both Brønsted and Lewis sites in parent zeolite and zeolites desilicated with NaOH and NaOH&TBAOH mixture determined in IR experiments with both Py and $NH_3$ (Table 3) were compared with the Al content from chemical analysis. The total concentrations of acid sites, (entries L+B in Table 3), determined with both probe molecules are close to the Al content obtained from the chemical analysis, validating the accuracy of our experimental procedure for the quantification of the acid sites. Additionally, since the total concentration of acid sites is consistent with the concentration of Al, it is suggested that each Al atom is able to form either Si(OH)Al group or highly dispersed Lewis acid site.

Desilication of zeolite resulted in the increase of concentration of both Brønsted and Lewis sites (the decrease of Si/Al) when comparing with parent zeolite due to the increase of the Al concentration in the treated materials, as generally accepted.

It is worth mentioning that in parent zeolite only ca. 65% of Al is engaged in the formation of the Si(OH)Al groups; the rest of Al exists as the electron acceptor extraframework species [32, 44]. However, this proportion decreases to 40% in the NaOH treated zeolite Beta, while is fully preserved (or even slightly increased) in the NaOH&TBAOH modified zeolite. These findings strongly support the less extensive destruction of zeolite framework in the presence of NaOH&TBAOH than of NaOH, as evidenced by XRD studies.

### *3.3.3. Lewis acid sites*

The nature of the acid sites was studied by low temperature CO adsorption. Narrow and well resolved bands of CO engaged into interaction with both Brønsted and Lewis sites appear in the region: 2135 - 2150 $cm^{-1}$. The spectra of CO adsorbed on the parent and desilicated zeolites Beta (Figure 7a) show three bands: the 2175 $cm^{-1}$ band of CO interacting with the Si(OH)Al groups, the 2190 $cm^{-1}$ band of CO bonded to extraframework aluminium species, and the 2230 $cm^{-1}$ band of CO interacting with Lewis sites formed by dehydroxylation [45]. The presence of the 2230 $cm^{-1}$ bands of higher intensities for the desilicated materials clearly evidences a significant contribution of the Lewis sites originating from the dehydroxylation process. Also, the intensity of the band at 2175 $cm^{-1}$ increases upon desilication processes. This could be attributed to the decrease of the Si/Al ratio of the zeolite Beta upon alkaline treatment. Then, the number of Brønsted and Lewis sites increases upon desilication. Notably, the largest increase of intensities of the bands attributed to CO adsorbed on Lewis sites was found for the sample treated with NaOH that also show the lowest crystallinity. The sample desilicated with NaOH&TBAOH shows an intermediate absorbance in the characteristic bands of CO bonded to Lewis sites. These results are in full agreement to the results of quantitative measurements with ammonia and pyridine (Table 3) and support the hypothesis of the formation of Lewis sites

### *3.3.4. The acid strength of the Si(OH)Al groups and of Lewis acid sites*

The information on the acid strength of the Si(OH)Al groups was provided from: (i) the frequencies of the IR band of free Si(OH)Al groups, (ii) the frequency shifts $\Delta\nu_{OH\cdots CO}$ of the band of the Si(OH)Al groups interacting with CO (Figure 7b) as well as (iii) from pyridine thermodesorption experiments. All the data presented in Table 3 evidenced the decrease of the acid strength of the Si(OH)Al groups upon desilication: the frequencies of the IR band of free Si(OH)Al groups increase and the frequency shift $\Delta\nu_{OH\ldots CO}$ decreases for desilicated materials. The same conclusion may be drawn from pyridine thermodesorption experiments, the procedure of which is given below. All acid sites were neutralized by pyridine and physisorbed molecules were subsequently removed by evacuation at 170 ºC. In the second step, desorption was carried out at 300 ºC to remove weakly bonded pyridine molecules. The ratio $A_{300}/A_{170}$, where $A_{170}$ and $A_{300}$ were the intensities of $PyH^+$ bands (1545 $cm^{-1}$) measured after each step of desorption, was taken as the measure of the acid strength of protonic sites. The $A_{300}/A_{170}$ values for desilicated zeolites are lower than for parent one evidencing the

decrease of the acid strength. Similar results were previously described for zeolites ZSM-5 of different Al contents [32].

This decrease of the acid strength of protonic sites can be related to the extraction of some Al atoms from zeolite in alkaline. The most likely, these Al atoms involved into formation of the most acidic Si(OH)Al groups are the less stable in tetrahedral framework positions of zeolite and in consequence, are extracted by alkali treatment in the first order. Such an interpretation was proposed in our earlier study of desilicated zeolite ZSM-5 [10].

The information on the acid strength of Lewis sites was also obtained in pyridine thermodesorption experiments following a similar procedure than for Brønsted sites. However, $A_{170}$ and $A_{300}$ were the intensities of the band pyridine coordinatively bonded to Lewis sites (1450 $cm^{-1}$). The $A_{300}/A_{170}$ values (Table 3) in desilicated zeolites are distinctly higher than in parent one evidencing the noticeable increase of the acid strength. This effect can be explained by considering the nature of Lewis sites. In parent zeolite Beta majority of the Lewis acid sites have origin in the extraframework Al atoms, which have been extracted during thermal decomposition of template. In the case of desilicated zeolites Beta, the formation some amorphous silica-alumina species and therefore having weak Lewis acidity can explain the presence of this high concentration of Lewis acid sites of relatively low acid strength.

The most of Lewis acid sites in desilicated zeolites were formed by the dehydroxylation of the protonic sites created by the reincorporation of Al atoms previously removed (together with Si) from zeolite during mesopore formation. The acid strength of both kinds of Lewis sites is considerably different. The sites originated from dehydroxylation are much more acidic than those being extraframework aluminium species. This was evidenced by higher frequency of the band of CO interacting with the respective sites (2230 and 2190 $cm^{-1}$). What is more, high contribution of strongly acidic Lewis sites results in an increase of the average acid strength of Lewis sites in desilicated zeolite as evidenced by the increase of $A_{300}/A_{170}$ values obtained from pyridine thermodesorption (Table 3).

### 3.4. Catalytic cracking performance of hierarchical Beta zeolites

The evaluation of hierarchical Beta zeolites in cracking reactions was performed with use of different feeds:1,3,5-tri-iso-propylbenzene (TIPB), *n*-decane and vacuum gas oil. It is expected that the activity of zeolite samples in cracking of TIPB molecules, which are not

able to penetrate the 12 MR channels, reveal the differences in accessibility of acid sites on the catalysts' surface. The influence of differences in intrinsic Brønsted acidity on catalytic cracking will be discussed with regard to *n*-decane cracking reactions, which are more demanding on the concentration and the strength of acid sites and is able to diffuse through the complete system of channels. Finally, the study is completed using a real FCC feed, since zeolite Beta is one of the proposed additives. Indeed, it has been claimed that zeolite Beta improves the yield to light olefins, while preserves the yield of gasoline. However, the major drawback of zeolite Beta as FCC additive is the fast deactivation due to coke formation [46]. The desilicated Beta zeolites with secondary system of mesopores are expected to overcome the limitations of typical microporous Beta zeolite. Catalytic cracking results were verified with regard to acidity IR data as well as to textural parameters.

### *3.4.1. Study of accessibility: TIPB cracking*

The total TIPB cracking conversion versus catalyst to oil ratio is shown in Figure 8. Also, Table 4 gives the first order kinetic activity for TIPB cracking on the zeolites Beta samples studied here. From these results, it is clear that NaOH&TBAOH desilicated samples gives the highest activity, while the parent zeolite Beta and NaOH desilicated solid give approximately the same conversion and kinetic constants. The best catalytic performance for TIPB on NaOH&TBAOH Beta can be related to the highest mesopore surface area and therefore, the better accessibility to molecules that cannot penetrates into the microporous such as the bulky TIPB molecules. The following catalyst in activity is the parent zeolite Beta despite of the very low external surface area (i.e. very low mesoporosity). This could be explained by considering that the acid sites in the parent material are fully zeolitic and therefore, showing the strongest acidity with a very high turnover frequency, resulting in a relatively high conversion of TIPB. Finally, NaOH desilicated Beta shows the lowest activity for TIPB cracking, even though very close to the parent zeolite. The low activity of NaOH treated material is attributed to the presence of amorphous silica-alumina, which is located at the outer part of the particle (as discussed above) and therefore, TIPB molecules react on relatively weak acid sites corresponding to amorphous silica-alumina [47, 48] resulting in a very low overall conversion. Then, from these results, it could be concluded that NaOH&TBAOH-zeolite Beta combines both features for having the best catalytic performance for large molecules conversions, on one hand very good accessibility due to the formation of mesoporosity during alkaline treatment, and on the other hand the presence of strong zeolitic Si-OH-Al acid sites, excluding the formation of amorphous silica-alumina,

being a true hierarchical meso- and microporous zeolite in which most of its active acid sites corresponds to zeolitic sites.

### *3.4.2. The cracking of n-decane molecule and the gas oil*

For the *n*-decane cracking the decisive factor is the density and the strength of acid sites of the bulk catalysts, since *n*-decane is able to diffuse through all the system of channels. As can be seen in Figure 9 and Table 4 the total conversion of *n*-decane is comparable for both parent and desilicated with NaOH&TBAOH what matches with IR acidity results (Table 3), while the sample desilicated with NaOH gives the lowest activity. This tendency fully agrees with our previous conclusion based on TIPB cracking results, that suggested the NaOH&TBAOH treated and the parent catalysts possess the most strong acid sites and therefore provides the highest catalytic activity, while the presence of amorphous silica-alumina in NaOH-treated zeolite Beta diminishes its averaged acid strength resulting in a lowering of its activity for *n*-decane cracking.

The observed selectivity during *n*-decane cracking gives very useful information about the acidity and diffusivity of reactant and products. NaOH&TBAOH treated zeolite Beta, that provides the shortest reaction path of the catalysts under study, gives the highest olefinicity in the $C_3$ and $C_4$ fraction (see Figure 9, $C_3=/C_3$, $C_4=/C_4$, $iC_4=/iC_4$ ratios), while produce less coke and dry gases. Indicating that less recracking is occurring in this material as could be expected by its improved diffusion properties. On the contrary, the NaOH-treated material gives the worst performance despite of containing also a large mesoporosity. However, as we discussed above, this is mostly formed by an amorphous silica-alumina lying on top of the zeolitic core. Then, *n*-decane must diffuse through a nearly inactive outer layer before reaching active sites with strong enough acidity for cracking this relatively refractory molecule. Then, the unique effect of this mesoporosity is increasing the catalyst tortuosity and this is clearly reflected in the highest $C_3/C_4$ ratio [49] and recracking and hydrogen transfer products (i.e. coke, paraffins, dry gases).

Finally, the results of gas oil cracking clearly show the benefit of having a true hierarchical meso- and microporous zeolite. Indeed, the NaOH&TBAOH treated zeolite Beta gives the highest total conversion of gasoil, but even more important, with the best selectivity towards the desired LCO fraction and having the highest olefinicity (Table 5, Figure 10). This could open a way for solving an open problem in FCC catalysts, which is to find catalysts that at the same time improve propylene yields, increasing LCO selectivity [50].

Our main conclusion is that the zeolite Beta treated with NaOH&TBAOH succeeds in all objectives: both the LCO and $C_3=/C_3$ ratios are higher than in case of parent and NaOH treated material (Table 5, Figure 10).

In addition, the higher yield to LCO obtained with zeolite Beta desilicated with NaOH&TBAOH confirms the ability of true hierarchical meso- and microporous zeolites to facilitate the accessibility of large molecules of VGO to the acid sites with subsequent diffusion of LCO produced without further secondary cracking. Moreover, the quality of the LCO, analysed by GCxGC (Table 6), is also optimum with a higher amount of paraffins and lower content in polyaromatics.

The present work unambiguously demonstrates the dependence of the catalytic performance with different feeds of desilicated zeolites Beta on their textural and acidic properties. The catalytic performance in TIPB as well as *n*-decane cracking is governed either by the accessibility or the acid strength of sites, respectively. Among studied zeolites, the most effective is the zeolite treated with NaOH&TBAOH, for which the development of secondary system of mesopores does not disturb the intrinsic acidity of zeolite.

## 4. CONCLUSIONS

In this work, it has been demonstrated that by a well-adjusted desilication procedure, combining the employ of NaOH and TBAOH as alkaline sources, it is possible to produce a hierarchical zeolite that combines mesoporosity and zeolitic microporosity without disturbing the intrinsic acidity of the parent zeolite. Both acid sites concentration and their strength have been reflected in catalytic activity and selectivity. As a result, an optimized catalyst with very high LCO and propylene selectivities during gas-oil cracking reaction has been achieved.

**Acknowledgment**

This work was supported by Grant No. 2011/01/B/ST5/00915 from the National Science Centre, Poland.

Also, M.C.I.L., J.M.T. and F.R. thanks financial support from the Spanish Ministry of Economy and Competitiveness through the Severo Ochoa program (SEV-2012-0267) as well as operating grants Consolider Ingenio Multicat (CSD-2009-00050) and MAT-2012-3856-C02-01

## References


[1] S. Kulprathipanja, *Zeolites in Industrial Separation and Catalysis.* s.l. : Wiley-VCH, Weinheim, 2010.

[2] M. Guisnet, J.-P. Gilson, *Zeolites for Cleaner Technologies, Catalytic Science Series vol. 3.* London : Imperial College Press, 2002.

[3] C.H. Christensen, K. Johannsen, E. Törnqvist, I. Schmidt, H. Topsøe, C.H.; Christensen, Mesoporous zeolite single crystal catalysts: Diffusion and catalysis in hierarchical zeolites. *Catal. Today.* 2007, 128, pp. 117-122.

[4] D. Verboekend, J. Pérez-Ramírez, Design of hierarchical zeolite catalysts by desilication. *Catal. Sci. Tech.*. 2011, 1 (6), pp. 879-890.

[5] Y. Tao, H. Kanoh, L. Abrams, K. Kaneko, Mesopore-Modified Zeolites: Preparation, Characterization, and Applications. *Chem. Rev.* 2006, 106 (3), pp. 896–910.

[6] J.C. Groen, J.C. Jansen, J.A. Moulijn, J. Pérez-Ramírez, Optimal Aluminum-Assisted Mesoporosity Development in MFI Zeolites by Desilication. *J. Phys. Chem. B.* 108 (35), pp. 13062-13065.

[7] D. Verboekend, S. Mitchell, M. Milina, J.C. Groen, J. Pérez-Ramírez, Full Compositional Flexibility in the Preparation of Mesoporous MFI Zeolites by Desilication. *J. Phys. Chem. C.* 115 (29), pp. 14193-14203.

[8] J. C. Groen, L. A. A. Peffer, J.A. Moulijn, J. Perez-Ramirez, Mechanism of Hierarchical Porosity Development in MFI Zeolites by Desilication: The Role of Aluminium as a Pore-Directing Agent. *Chem. Eur. J.* 2005, 11, pp. 4983-4994.

[9] D. Verboekend, J. Pérez-Ramírez, Desilication Mechanism Revisited: Highly Mesoporous All-Silica Zeolites Enabled Through Pore-Directing Agents. *Chem. Eur. J.* 2011, 17, pp. 1137-1147.

[10] K. Sadowska, K. Góra-Marek, M. Drozdek, P. Kuśtrowski, J. Datka, J. Martinez Triguero, F. Rey, Desilication of highly siliceous zeolite ZSM-5 with NaOH and NaOH/tetrabutylammonium hydroxide. *Microporous Mesoporous Mater.* 2013, 168, pp. 195–205.

[11] J. C. Groen, L. A. A. Peffer, J.A. Moulijn, J. Pérez-Ramírez, Desilication: On the controlled generation of mesoporosity in MFI zeolites. *J. Mater. Chem.* 2006, 6, pp. 2121-2131.

[12] R. Caicedo-Realpe, J. Pérez-Ramírez, Mesoporous ZSM-5 zeolites prepared by a two-step route comprising sodium aluminate and acid treatments. *Microporous Mesoporous Mater.* 2010, 128, pp. 91–100.

[13] X. Wei, P.G. Smirniotis, Development and characterization of mesoporosity in ZSM-12 by desilication. *Microporous Mesoporous Mater.* 2006, 97, pp. 97–106.

[14] J.C. Groen, T. Sano, L. A. A. Moulijn, J. Pérez-Ramírez, Alkaline-mediated mesoporous mordenite zeolites for acid-catalyzed conversions. *J. Catal.* 2007, 251, pp. 21–27.

[15] A.N.C. van Laak, R.W. Gosselink, S.L. Sagala, J. D. Meeldijk, P.E. de Jongh, K.P. de Jong, Alkaline treatment on commercially available aluminum rich mordenite. *Appl. Catal. A.* 2010, 382 (1), pp. 65-72.

[16] D. Verboekend, R. Caicedo-Realpe, A. Bonilla, M. Santiago, J. Pérez-Ramírez, Properties and Functions of Hierarchical Ferrierite Zeolites Obtained by Sequential Post-synthesis treatments. *Chem. Mater.* 2010, 22 (16), pp. 4679-4689.

[17] A. Bonilla, D. Baudouin, J. Pérez-Ramírez, Desilication of ferrierite zeolite for porosity generation and improved effectiveness in polyethylene pyrolysis. *J. Catal.* 2009, 265, pp. 170–180.

[18] K. P. de Jong, J.Zečević, H. Friedrich, P. E.de Jongh, M.Bulut, S. van Donk, R. Kenmogne, A. Finiels, V. Hulea, F. Fajula, Zeolite Y Crystals with Trimodal Porosity as Ideal Hydrocracking Catalysts. *Angew. Chem. Int. Ed.*. 2010, 49 (52), pp. 10074-10078.

[19] D. Verboekend, G; Vilé, J. Pérez-Ramírez, Mesopore Formation in USY and Beta Zeolites by Base Leaching: Selection Criteria and Optimization of Pore-Directing Agents. *Cryst. Growth Des.* 2012, 12, pp. 3123-3132.

[20] J.C. Groen, S. Abello, L.A. Villaescusa, J. Perez-Ramirez, Mesoporous beta zeolite obtained by desilication. *Microporous Mesoporous Mater.* 2008, 114, pp. 93-102.

[21] J.M. Newsam, M.M.J. Treacy, W.T. Koetsier, C.B. de Gruyter, Structural characterization of zeolite beta. *Proc. R. Soc. London, Ser. A.* 1988, 420, pp. 375-405.

[22] J.B. Higgins, R.B. LaPierre, J.L. Schlenker, A.C. Rohrman, J.D. Wood, G.T. Kerr, W.J. Rohrbaugh, The framework topology of zeolite beta. *Zeolites.* 1988, 8, pp. 446-452.

[23] E. Bourgeat-Lami, P. Massiani, F. Di Renzo, F. Fajula, T. Des Courieres, Stability of the tetrahedral aluminium sites in zeolite beta. *Catal. Lett.* 1990, 5, pp. 265-272.

[24] S. Svelle, L. Sommer, K. Barbera, P.N.R. Vennestrøm, U. Olsbye, K.P. Lillerud, S. Bordiga, Y.H. Pan, P. Beato, How defects and crystal morphology control the effects of desilication. *Catal. Today.* 2011, 168 (1), pp. 38-47.

[25] C. Martínez, D. Verboekend, J. Pérez-Ramírez, A. Corma, Stabilized hierarchical USY zeolite catalysts for simultaneous increase in diesel and LPG olefinicity during catalytic cracking. *Catal. Sci. Tech.*. 2013, 3 (4), pp. 972-981.

[26] E.F. Iliopoulou, S.D. Stefanidis, K.G. Kalogiannis, A.A. Lappas, J. Martinez-Triguero, M.T. Navarro, A.L. Chica, F. Rey, Mesopore-modified mordenites as catalysts for catalytic

pyrolysis of biomass and cracking of vacuum gasoil processes. *Green Chem.* 2013, 15 (6), pp. 1647-1658.

[27] N.Y. Chen, A.Y. Kam, C.R. Kennedy, A.B. Ketkar, D.M. Nace, *US 4740292*, 1988.

[28] L. Bonetto, M.A. Camblor, A. Corma, J. Pérez-Pariente, Optimization of zeolite beta in cracking catalysts. Influence of crystallite size. *Appl. Catal. A:* 1992, 82, pp. 37-50.

[29] L. Bonetto, A. Corma, E. Herrero, Beta Zeolite as Catalyst or Catalyst Additive for the Production of Olefins During Cracking of Gasoil. (Eds.) R. Higgins, J.B. Treacy, M.M.J. Von Ballmoos, *Proceedings from the 9th International Zeolite Conference I and II.* Boston: Butterworth-Heinemann, 1993, pp. 639-646.

[30] W. Makowski, B. Gil, D. Majda, Characterization of acidity and porosity of zeolite catalysts by the equilibrated thermodesorption of n-hexane and n-nonane. *Catal. Lett.* 2008, 120 (1-2), pp. 154-160.

[31] W. Makowski, Ł. Ogorzałek, Determination of the adsorption heat of n-hexane and n-heptane on zeolites beta, L, 5A, 13X, Y and ZSM-5 by means of quasi-equilibrated temperature-programmed desorption and adsorption (QE-TPDA). *Thermochim. Acta.* 2007, 465 (1-2), pp. 30-39.

[32] K. Sadowska, K. Góra-Marek, J. Datka, Hierarchic zeolites studied by IR spectroscopy: Acid properties of zeolite ZSM-5 desilicated with NaOH and NaOH/tetrabutylamine hydroxide. *Vib. Spectrosc.* 2012, 63, pp. 418-425.

[33] J. Datka, K. Góra-Marek, IR studies of the formation of ammonia dimers in zeolites TON. *Catal. Today.* 2006, 114 (2-3), pp. 205-210.

[34] A. Corma, J. Martínez-Triguero, Kinetics of gasoil cracking and catalyst decay on SAPO-37 and USY molecular sieves. *Appl. Catal. A.* 1994, 118 (2), pp. 153-162.

[35] A. Corma, F. Melo, J. Prieto, *ES 2 011 993,* 1989.

[36] Y. Mathieu, A. Corma, M. Echard, M. Bories, Single and combined effects of Bottom Cracking (BCA) and Propylene Booster (PBA) separate particles additives addition to a Fluid Catalytic Cracking (FCC) catalyst on the FCC product distribution and quality. *Appl. Catal. A.* 2012, 439-440, pp. 57-73.

[37] M.M. Helmkamp, M.E. Davis, Synthesis of porous silicates. *Annu. Rev. Mater. Sci.*. 1995, 25, pp. 161-192.

[38] X. Li, D.F. Shantz, PFG NMR Investigations of Tetraalkylammonium-Silica Mixtures. *J Phys Chem C.* 2010, 114, pp. 8449-8458.

[39] J. Pérez-Ramírez, S. Abelló, A. Bonilla, J.C. Groen, Tailored mesoporosity development in zeolite crystals by partial detemplation and desilication. *Adv. Funct. Mater.*. 2009, 19 (1), pp. 164-172.

[40] S. Abelló, A. Bonilla, J. Pérez-Ramírez, Mesoporous ZSM-5 zeolite catalysts prepared by desilication with organic hydroxides and comparison with NaOH leaching. *Appl. Catal. A.* 2009, 364 (1-2), pp. 191-198.

[41] K. Sadowska, A. Wach, Z. Olejniczak, P. Kuśtrowski, J. Datka, Hierarchic zeolites: Zeolite ZSM-5 desilicated with NaOH and NaOH/tetrabutylamine hydroxide. *Microporous Mesoporous Mater.* 2013, 167, pp. 82-88.

[42] W. Makowski, M. Mańko, A. Dudek, K. Mlekodaj, Application of quasi-equilibrated thermodesorption of hexane and cyclohexane for characterization of porosity of zeolites and ordered mesoporous silicas. *Adsorpt.* 2013, 19 (2-4), pp. 537-544.

[43] W. Makowski, L. Chmielarz, P. Kuśtrowski, Determination of the pore size distribution of mesoporous silicas by means of quasi-equilibrated thermodesorption of n-nonane. *Microporous Mesoporous Mater.* 2009, 120 (3), pp. 257-262.

[44] C.J. van Oers, K. Góra-Marek, K. Sadowska, M. Mertens, V. Meynen, J. Datka, P. Cool, In situ IR spectroscopic study to reveal the impact of the synthesis conditions of zeolite β nanoparticles on the acidic properties of the resulting zeolite. *Chem. Eng. J.* 2014, 237, pp. 372-379.

[45] J.P. Marques, I. Gener, P. Ayrault, J.C. Bordado, J.M. Lopes, F.R. Ribeiro, M. Guisnet, Dealumination of HBEA zeolite by steaming and acid leaching: Distribution of the various aluminic species and identification of the hydroxyl groups. *Comptes Rendus Chimie.* 2005, 8 (3-4), pp. 399-410.

[46] A. Corma, P.J. Miguel, A.V. Orchille, Influence of hydrocarbon chain length and zeolite structure on the catalyst activity and deactivation for n-alkanes cracking. *Appl. Catal. A.* 1994, 117, pp. 29-40.

[47] A. Corma, V. Fornes, L. Forni, F. Marquez, J. Martinez Triguero, D. Moscottiy, 2,6-Di-Tert-Butyl-Pyridine as a Probe Molecule to Measure External Acidity of Zeolites. *J. Catal.* 1998, 179, pp. 451-458.

[48] E. Aguiar, S. Falabella, M.L. Murta Valle, M.P. Silva, D.F. Silva, Influence of external surface area of rare-earth containing Y zeolites on the cracking of 1,3,5-triisopropylbenzene. *Zeolites.* 1995, 15, pp. 620-623.

[49] A. Corma, J. Martínez-Triguero, S. Valencia, E. Benazzi, S. Lacombe, IM-5: A highly thermal and hydrothermal shape-selective cracking zeolite. *J. Catal.* 2002, 206 (1), pp. 125-133.

[50] P. K. Niccum, Maximize diesel production in an FCC-centered refinery, Part 1. *Hydrocarbon Process.* 2012, 91 (9).

FIGURES CAPTIONS

**Figure 1.** X-ray diffraction patterns of the parent zeolite Beta and zeolite treated with 0.2 M NaOH and 0.2 M NaOH&TBAOH mixture.

**Figure 2.** $^{29}$Si MAS NMR spectra of the parent zeolite Beta and zeolite desilicated with 0.2 M NaOH and 0.2 M NaOH&TBAOH mixture.

**Figure 3.** Adsorption isotherms of $N_2$ and BJH pore size distribution (inset) of the parent zeolite Beta and zeolite treated with 0.2 M NaOH and 0.2 M NaOH&TBAOH mixture.

**Figure 4.** TEM microphotographs of the parent zeolite Beta (a/500 nm and a'/200 nm) and zeolite treated with 0.2 M NaOH (b/500 nm and b'/200 nm) and 0.2 M NaOH&TBAOH mixture (c/500 nm and c'/200 nm).

**Figure 5.**

**a –** QE-TPDA profiles of *n*-hexane on Beta zeolites

**b –** QE-TPDA profiles of *n*-nonane on Beta zeolites

**c –** Mesopore size distribution calculated for Beta zeolites from QE-TPDA profiles of *n*-nonane for the parent zeolite Beta and zeolite treated with 0.2 M NaOH and 0.2 M NaOH&TBAOH mixture.

**Figure 6.** The IR spectra in the region of OH groups vibration of parent zeolite Beta and zeolites treated with 0.2 M NaOH and 0.2 M NaOH&TBAOH mixture.

**Figure 7.**The spectra of CO sorbed at -100 $^{o}$C in parent zeolite and zeolite treated with NaOH and NaOH&TBAOH mixture in the C≡O vibrations region (a) and in the region of stretching hydroxyls vibration (b).

**Figure 8.** Total conversion and selectivities in the cracking of TIPB at 500 $^{o}$C and 60 s time on stream over parent and hierarchical Beta zeolites.

**Figure 9.** Total conversion and selectivities in the cracking of *n*-decane at 500 $^{o}$C and 60 s time on stream over parent and hierarchical Beta zeolites.

**Figure 10.** Total conversion and selectivities in the cracking of vacuum gas oil at 520 $^{o}$C and 30 s time on stream over parent and hierarchical Beta zeolites.

**Table 1.** The relative crystallinity values (%Cryst) derived from XRD, the composition determined by chemical analysis $(Si/Al)_{bulk}$, the composition of surface zone from XPS measurements $(Si/Al)_{surf}$, the $(Si/Al)_{surf}/(Si/Al)_{bulk}$ factor, the % of Si and Al extracted during desilication.

| **zeolite Beta** | **%Cryst** | $(\boldsymbol{Si/Al})_{\boldsymbol{bulk}}$ | $(\boldsymbol{Si/Al})_{\boldsymbol{surf}}$ | $\frac{(\boldsymbol{Si/Al})_{\boldsymbol{surf}}}{(\boldsymbol{Si/Al})_{\boldsymbol{bulk}}}$ | **% $Si_{ext}$** | **% $Al_{ext}$** |
|---|---|---|---|---|---|---|
| **parent** | 100 | 22 | 27 | 1.23 | - | - |
| **NaOH** | 66 | 13 | 10 | 0.77 | 52 | 2.3 |
| **NaOH&TBAOH** | 100 | 16 | 15 | 0.94 | 41 | 1.5 |

**Table 2.** The textural parameters from low temperature $N_2$ adsorption and from QE-TPDA of hydrocarbons for parent zeolite Beta and zeolites desilicated with NaOH and NaOH&TBAOH mixture.

| zeolite Beta | $S_{BET}$ [$m^2\ g^{-1}$] | $S_{meso}$ [$m^2\ g^{-1}$] | $V_{micro}$[$cm^3\ g^{-1}$] | | $V_{meso}$[$cm^3\ g^{-1}$] | | $D_{meso}$[nm] | |
|---|---|---|---|---|---|---|---|---|
| | | | ***n*-hexane** | **$N_2$** | ***n*-nonane** | **$N_2$** | ***n*-nonane** | **$N_2$** |
| **parent** | 567 | 44 | 0.18 | 0.18 | 0.09 | 0.06 | - | - |
| **NaOH** | 668 | 510 | 0.15 (0.13*) | 0.10 | 0.53 | 0.40 | 5.3 | 5.5 |
| **NaOH&TBAOH** | 793 | 468 | 0.22 (0.18*) | 0.14 | 0.35 | 0.35 | 4.1 | 3.8 |

**values corrected for the low temperature desorption contribution.*

**Table 3.** The composition of the parent Beta zeolite and hierarchical ones determined by chemical analysis $(Si/Al)_{bulk}$, the concentration of Al atoms from chemical analysis, the concentration of Brønsted (B) and Lewis acid sites (L) from IR spectroscopy measurements with pyridine and ammonia as probe molecules as well as the acid strength of the Si(OH)Al groups and Lewis acid sites derived from IR studies of pyridine thermodesorption and low temperature CO sorption (expressed by $\Delta\nu_{O\text{-}H\cdots CO}$).

| **zeolite Beta** | $(Si/Al)_{bulk}$ | **Al [µmol·g$^{-1}$]** | **Py [µmol·g$^{-1}$]** | | | **$NH_3$ [µmol·g$^{-1}$]** | | | **Strength of Brønsted a.c.** | | | **Strength of Lewis a.c.** |
|---|---|---|---|---|---|---|---|---|---|---|---|---|
| | | | **B** | **L** | **L+B** | **B** | **L** | **L+B** | $\nu_{OH}$ **[cm$^{-1}$]** | $\Delta\nu_{OH\cdots CO}$ **[cm$^{-1}$]** | $\frac{A_{300}}{A_{170}}$ | $\frac{A_{300}}{A_{170}}$ |
| **parent** | 22 | 675 | 395 | 220 | 615 | 410 | 200 | 610 | 3604 | 309 | 1 | 0.31 |
| **NaOH** | 13 | 1100 | 450 | 650 | 1100 | 500 | 600 | 1100 | 3612 | 301 | 0.8 | 1.00 |
| **NaOH&TBAOH** | 16 | 975 | 650 | 330 | 980 | 670 | 300 | 970 | 3609 | 303 | 0.9 | 0.85 |

**Table 4.** The first-order kinetic rate constants for TIPB ($K_{TIPB}$), *n*-decane ($K_{n\text{-decane}}$) and the second-order kinetic rate constants for vacuum gas oil ($K_{gas\ oil}$) cracking reactions.

| zeolite Beta | Experimental kinetic rate constants [$g_{oil}\ g_{cat}^{-1}\ s^{-1}$] | | |
|---|---|---|---|
| | $K_{TIPB}$ | $K_{n\text{-decane}}$ | $K_{gas\ oil}$ |
| **parent** | 0.107 | 0.108 | 0.041 |
| **NaOH** | 0.104 | 0.071 | 0.026 |
| **NaOH&TBAOH** | 0.137 | 0.099 | 0.048 |

**Table 5.** Interpolated yields and olefinicity ratios at 75wt% of Total Conversion in the catalytic cracking of VGO at 500ºC and Time On Stream of 30s.

| zeolite Beta | parent | NaOH | NaOH&TBAOH |
|---|---|---|---|
| **cat/oil ratio (wt/wt)** | 2.62 | 3.26 | 2.27 |
| **Yields (wt%)** | | | |
| **gasoline** | 19.12 | 26.46 | 22.46 |
| **LCO** | 20.77 | 10.17 | 25.38 |
| **gases $C_1$-$C_4$** | 29.24 | 32.68 | 22.94 |
| **coke** | 5.87 | 5.69 | 4.23 |
| **hydrogen** | 0.04 | 0.05 | 0.04 |
| **methane** | 0.92 | 1.06 | 0.87 |
| **ethane $C_2$** | 0.80 | 0.87 | 0.73 |
| **ethylene $C_2$=** | 1.51 | 1.72 | 1.14 |
| **propane $C_3$** | 4.23 | 3.02 | 1.90 |
| **propylene $C_3$=** | 6.18 | 8.31 | 5.61 |
| **isobutane** | 6.02 | 6.01 | 4.13 |
| ***n*-butane** | 2.26 | 1.81 | 1.22 |
| ***trans*-2-butene** | 1.69 | 2.27 | 1.67 |
| **but-1-ene** | 1.29 | 1.76 | 1.30 |
| **isobutylene** | 3.08 | 4.11 | 3.10 |
| ***cis*-2-butene** | 1.23 | 1.67 | 1.22 |
| **Ratios (wt/wt)** | | | |
| **$C_4$=/$C_4$** | 0.88 | 1.25 | 1.36 |
| **$C_3$=/$C_3$** | 1.46 | 2.75 | 2.96 |
| **($C_1$+$C_2$)/*i*$C_4$** | 0.54 | 0.61 | 0.66 |
| **$C_3$/$C_4$** | 0.67 | 0.64 | 0.59 |

**Table 6.** The GCxGC analysis of LCO fraction ($C_{12}$-$C_{20}$) in the catalytic cracking of VGO at 500ºC and Time On Stream of 30s on parent and desilicated samples at 75wt% of conversion level

| zeolite Beta | parent | NaOH | NaOH&TBAOH |
|---|---|---|---|
| **LCO yield** | 20.77 | 10.17 | 25.38 |
| **yields (wt%)** | | | |
| **saturates** | 6.94 | 3.19 | 9.01 |
| **monoaromatics** | 3.89 | 2.12 | 5.11 |
| **diaromatics** | 6.28 | 3.21 | 6.93 |
| **triaromatics** | 3.65 | 1.66 | 4.33 |
| **selectivity (wt%)** | | | |
| **saturates** | 33.43 | 31.35 | 35.51 |
| **monoaromatics** | 18.75 | 20.80 | 20.12 |
| **diaromatics** | 30.25 | 31.54 | 27.31 |
| **triaromatics** | 17.57 | 16.31 | 17.06 |

Figure 1.

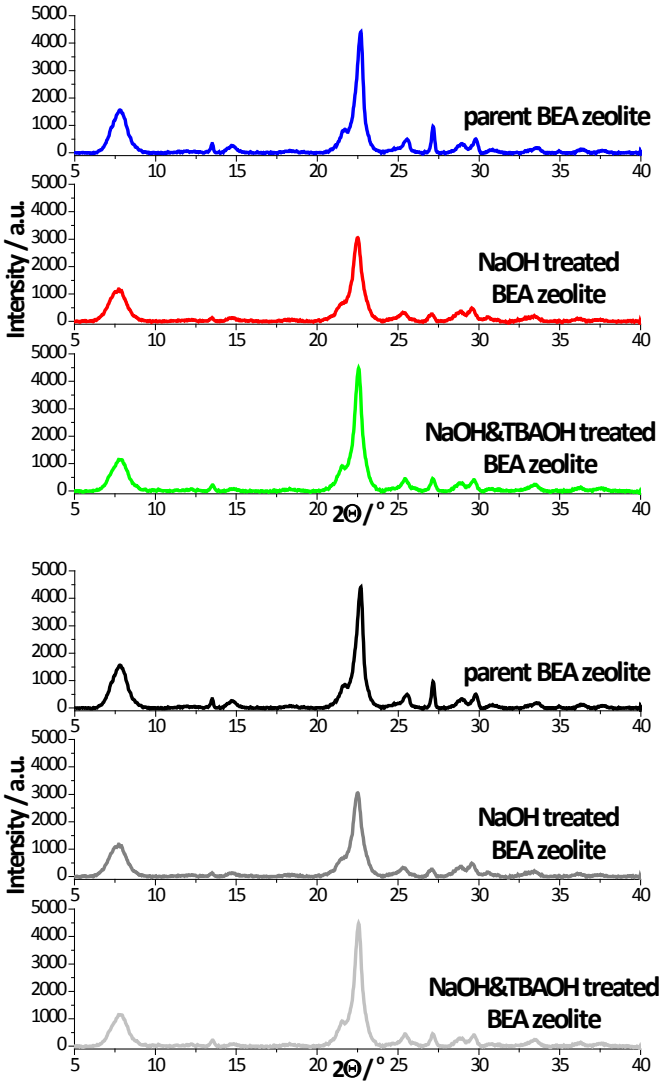
parent BEA zeolite
NaOH treated BEA zeolite
NaOH&TBAOH treated BEA zeolite
Intensity / a.u.
2Θ / °
parent BEA zeolite
NaOH treated BEA zeolite
NaOH&TBAOH treated BEA zeolite
Intensity / a.u.
2Θ / °

Figure 2.

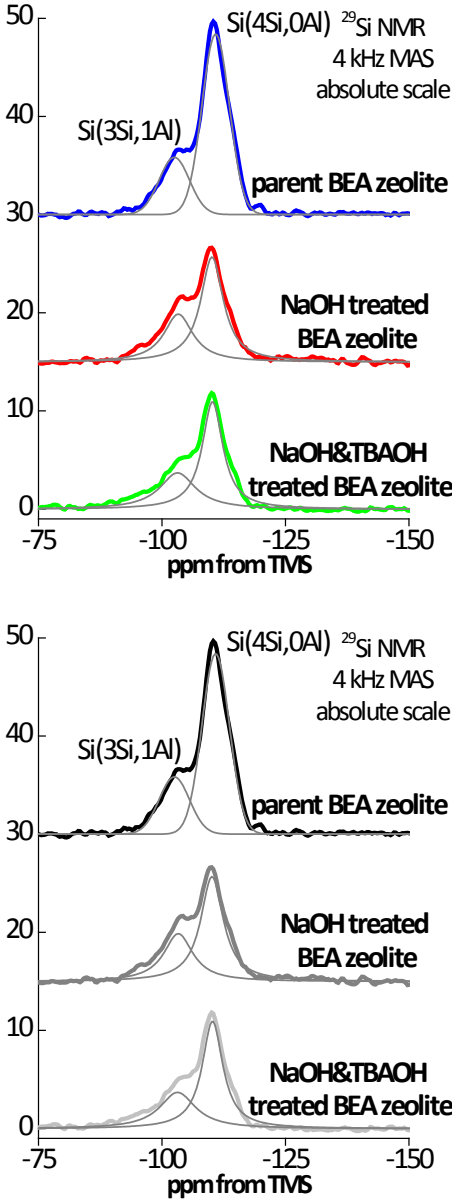
Si(4Si,0Al) 29Si NMR
4 kHz MAS
absolute scale
Si(3Si,1Al)
parent BEA zeolite
NaOH treated
BEA zeolite
NaOH&TBAOH
treated BEA zeolite
50
40
30
20
10
0
-75
-100
-125
-150
ppm from TMS
Si(4Si,0Al) 29Si NMR
4 kHz MAS
absolute scale
Si(3Si,1Al)
parent BEA zeolite
NaOH treated
BEA zeolite
NaOH&TBAOH
treated BEA zeolite
50
40
30
20
10
0
-75
-100
-125
-150
ppm from TMS

Figure 3.

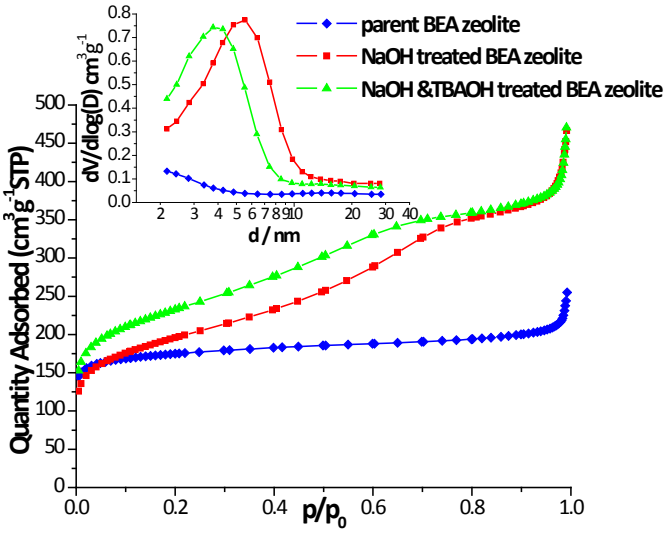
parent BEA zeolite
NaOH treated BEA zeolite
NaOH &TBAOH treated BEA zeolite
Quantity Adsorbed (cm3g-1STP)
p/p0
dV/dlog(D) cm3g-1
d / nm

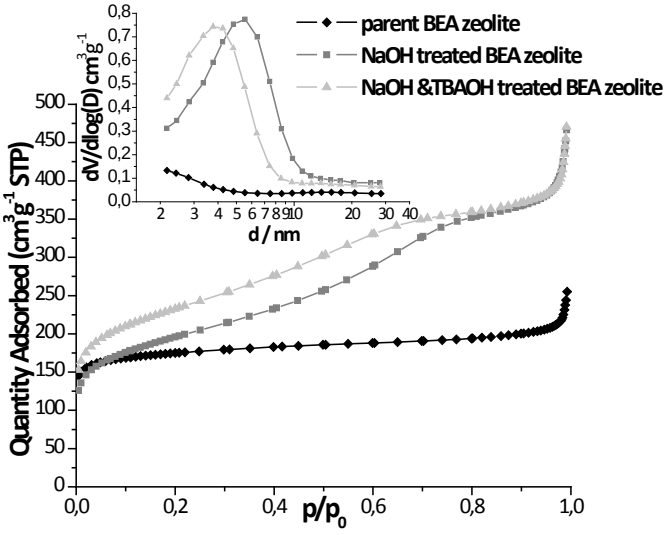
parent BEA zeolite
NaOH treated BEA zeolite
NaOH &TBAOH treated BEA zeolite
Quantity Adsorbed (cm3g-1 STP)
p/p0
dV/dlog(D) cm3g-1
d / nm

Figure 4.

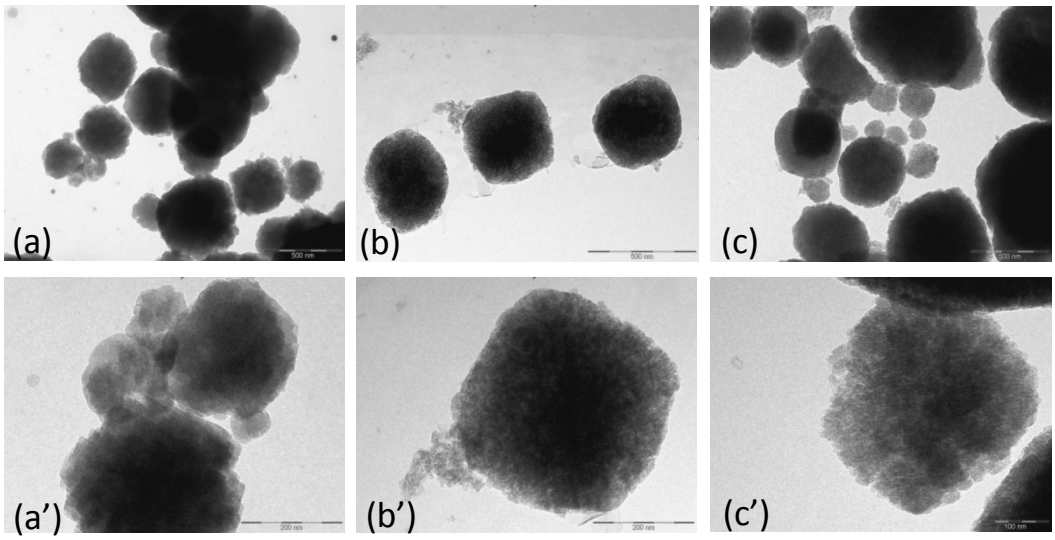

Figure 5.

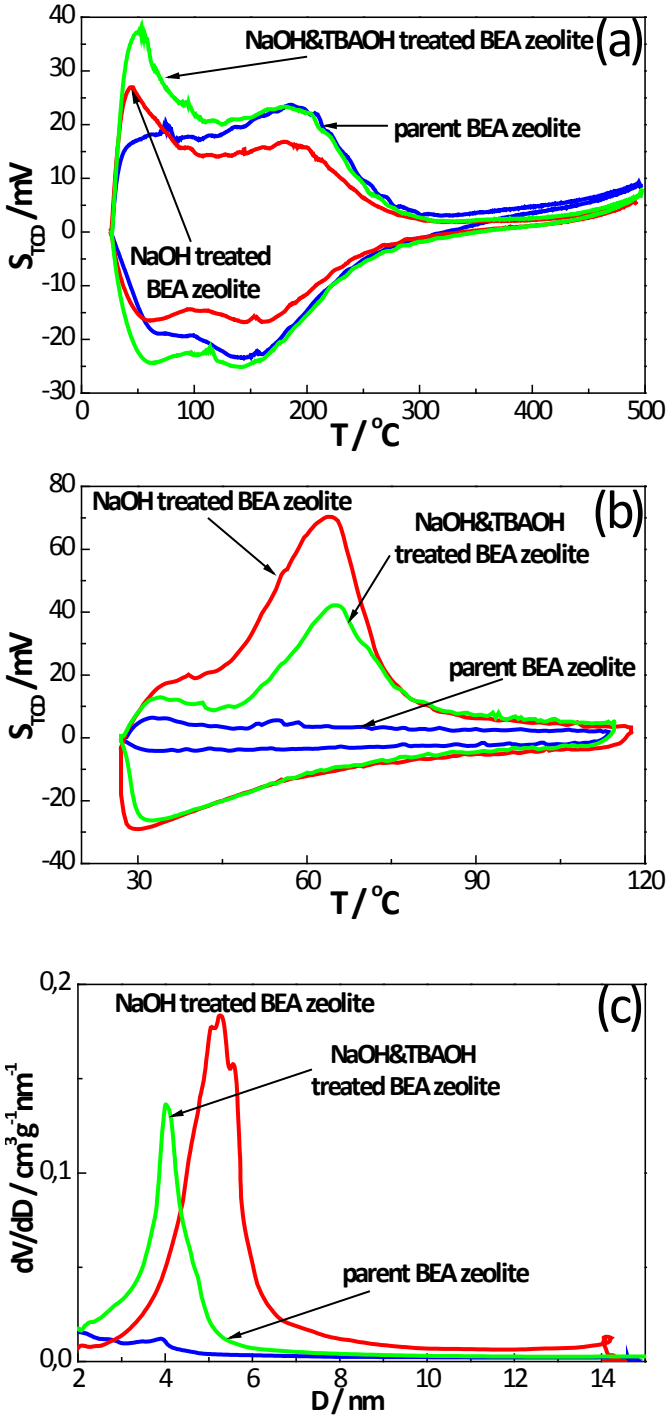
NaOH&TBAOH treated BEA zeolite
(a)
parent BEA zeolite
NaOH treated
BEA zeolite
$S_{TCD}$ /mV
T / °C
NaOH treated BEA zeolite
NaOH&TBAOH
treated BEA zeolite
(b)
parent BEA zeolite
$S_{TCD}$ /mV
T / °C
NaOH treated BEA zeolite
NaOH&TBAOH
treated BEA zeolite
(c)
parent BEA zeolite
dV/dD / cm$^3$g$^{-1}$nm$^{-1}$
D / nm

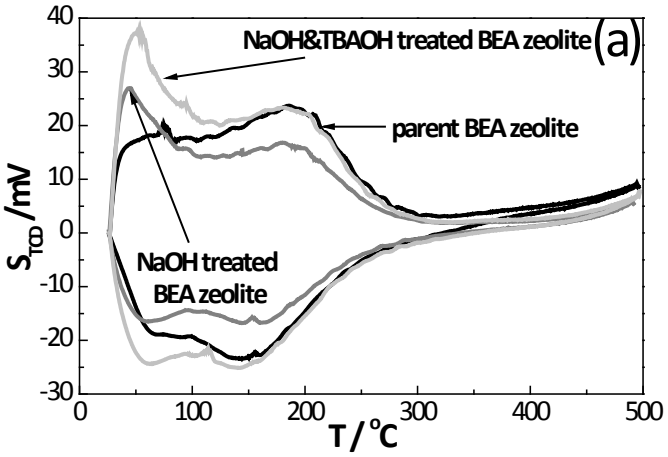
NaOH&TBAOH treated BEA zeolite
(a)
parent BEA zeolite
NaOH treated
BEA zeolite
$S_{TCD}$ /mV
T / °C

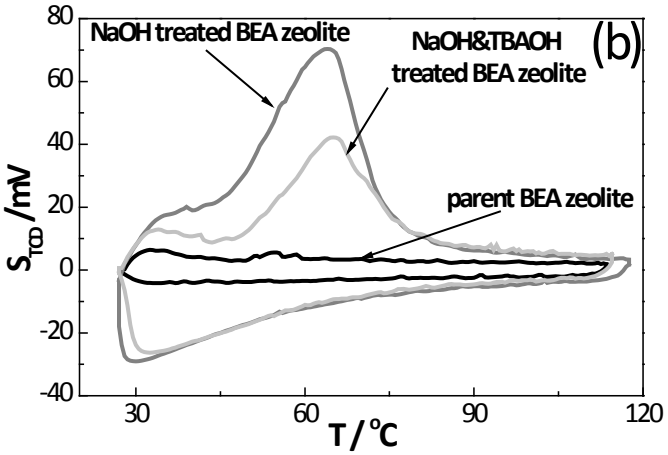
NaOH treated BEA zeolite
NaOH&TBAOH
treated BEA zeolite
(b)
parent BEA zeolite
$S_{TCD}$ /mV
T / °C

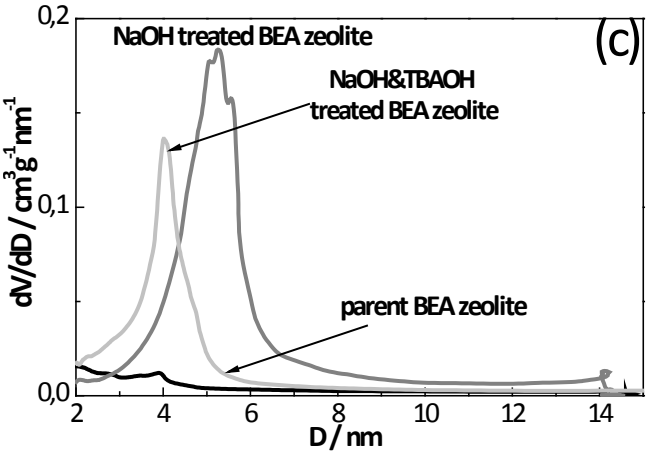
NaOH treated BEA zeolite
(c)
NaOH&TBAOH
treated BEA zeolite
parent BEA zeolite
dV/dD / cm³g⁻¹nm⁻¹
D / nm

Figure 6.

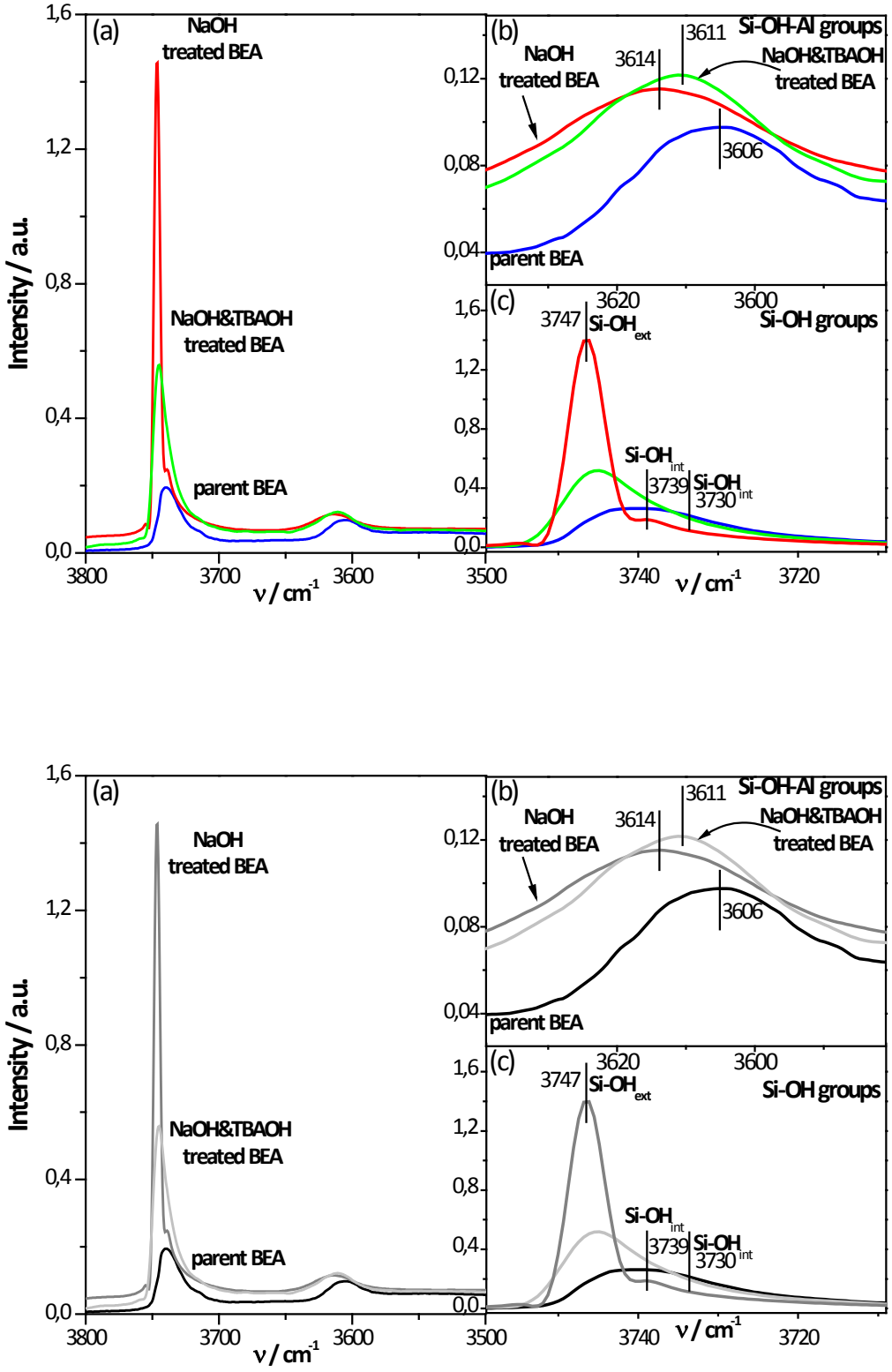
(a)
NaOH
treated BEA
NaOH&TBAOH
treated BEA
parent BEA
Intensity / a.u.
ν / cm-1
(b)
Si-OH-Al groups
3611
3614
NaOH
treated BEA
NaOH&TBAOH
treated BEA
3606
parent BEA
(c)
3747
Si-OHext
3620
3600
Si-OH groups
Si-OHint
3739
Si-OHint
3730

Figure 7.

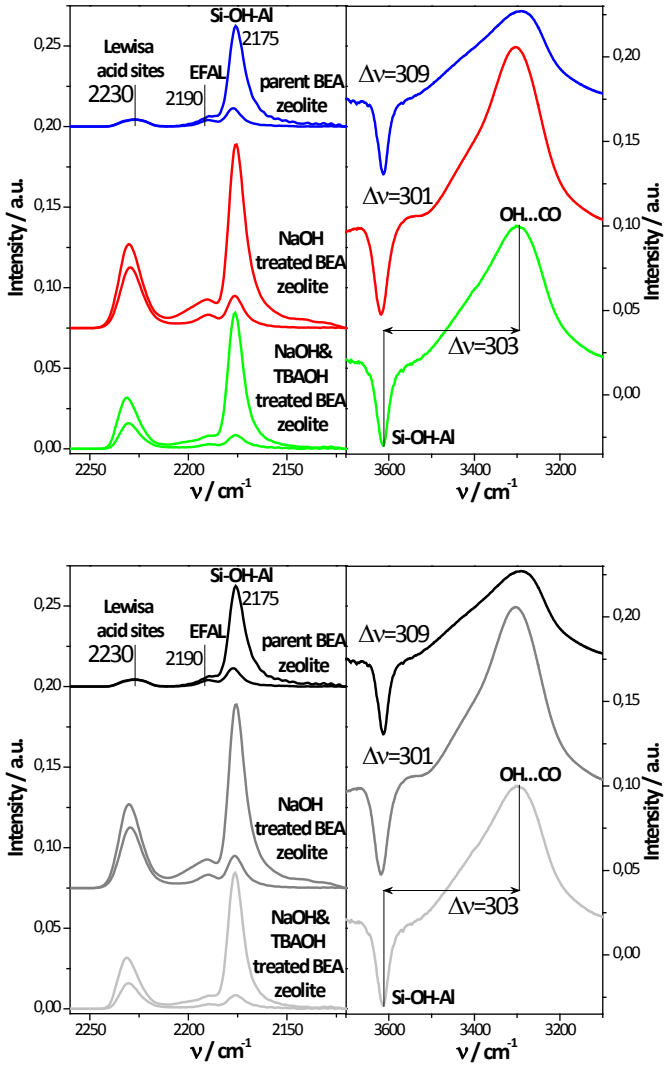
Si-OH-Al
2175
Lewisa
acid sites
2230
EFAL
2190
parent BEA
zeolite
NaOH
treated BEA
zeolite
NaOH&
TBAOH
treated BEA
zeolite
Δν=309
Δν=301
OH...CO
Δν=303
Si-OH-Al
Intensity / a.u.
ν / cm-1

Figure 8.

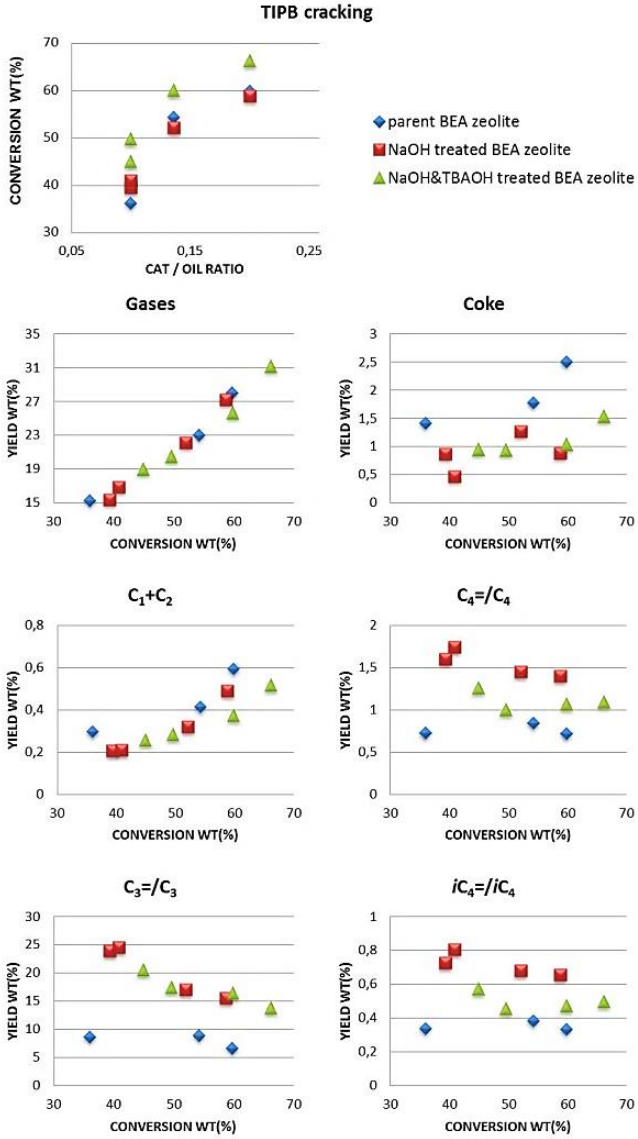
TIPB cracking
CONVERSION WT(%)
CAT / OIL RATIO
parent BEA zeolite
NaOH treated BEA zeolite
NaOH&TBAOH treated BEA zeolite
Gases
Coke
$C_1+C_2$
$C_4=/C_4$
$C_3=/C_3$
$iC_4=/iC_4$
YIELD WT(%)
CONVERSION WT(%)

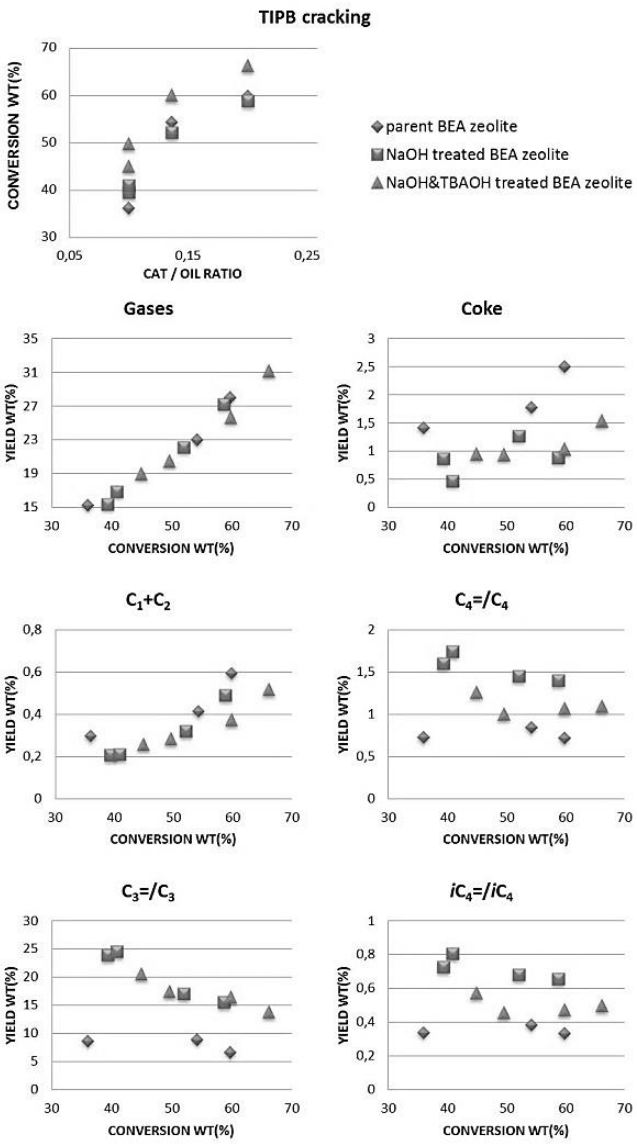
TIPB cracking
CONVERSION WT(%)
CAT / OIL RATIO
parent BEA zeolite
NaOH treated BEA zeolite
NaOH&TBAOH treated BEA zeolite
Gases
Coke
$C_1+C_2$
$C_4=/C_4$
$C_3=/C_3$
$iC_4=/iC_4$
YIELD WT(%)
CONVERSION WT(%)

Figure 9.

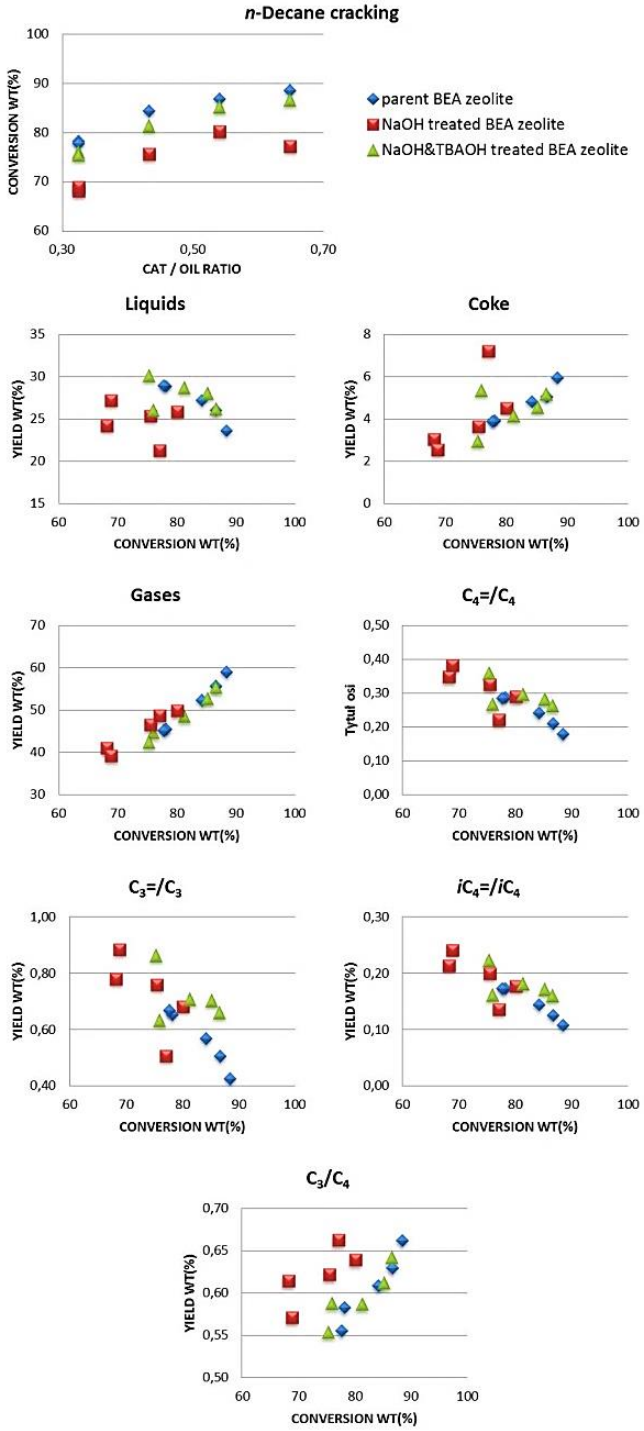
n-Decane cracking
CONVERSION WT(%)
CAT / OIL RATIO
parent BEA zeolite
NaOH treated BEA zeolite
NaOH&TBAOH treated BEA zeolite
Liquids
Coke
Gases
C4=/C4
C3=/C3
iC4=/iC4
C3/C4
YIELD WT(%)
Tytul osi
CONVERSION WT(%)

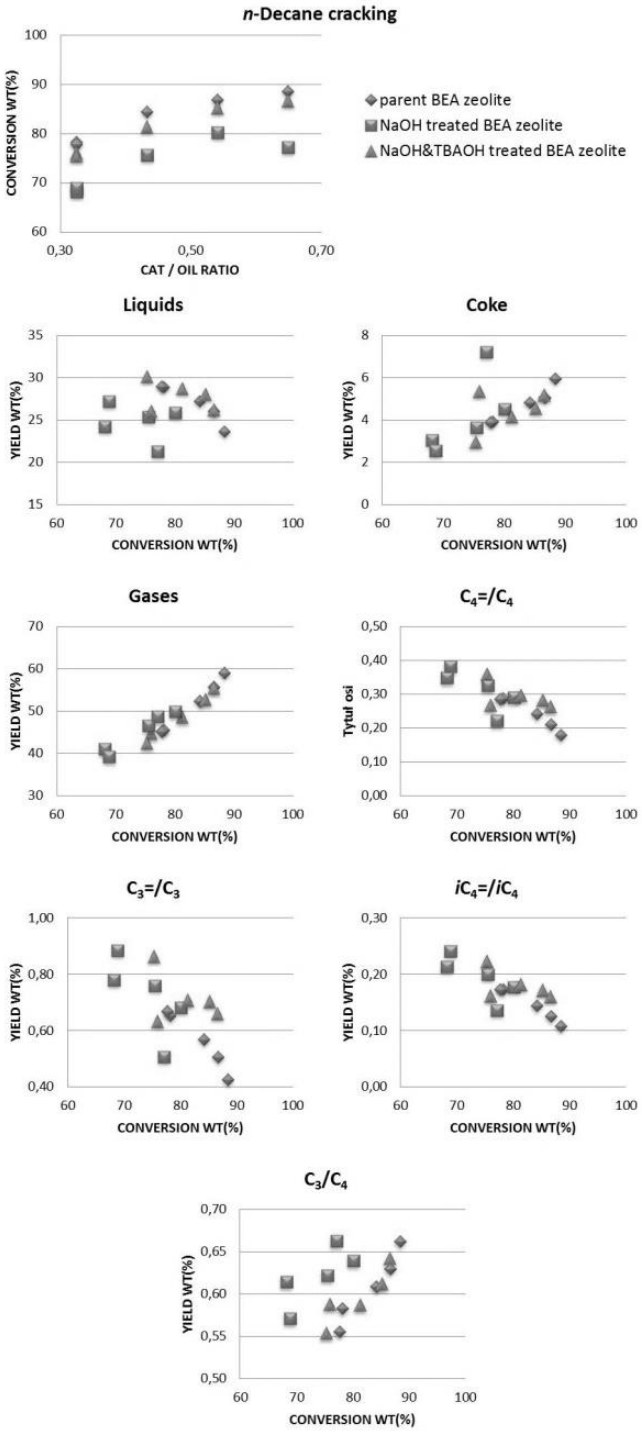
n-Decane cracking
CONVERSION WT(%)
CAT / OIL RATIO
parent BEA zeolite
NaOH treated BEA zeolite
NaOH&TBAOH treated BEA zeolite
Liquids
Coke
Gases
C4=/C4
C3=/C3
iC4=/iC4
C3/C4
YIELD WT(%)
Tytuł osi
CONVERSION WT(%)

Figure 10.

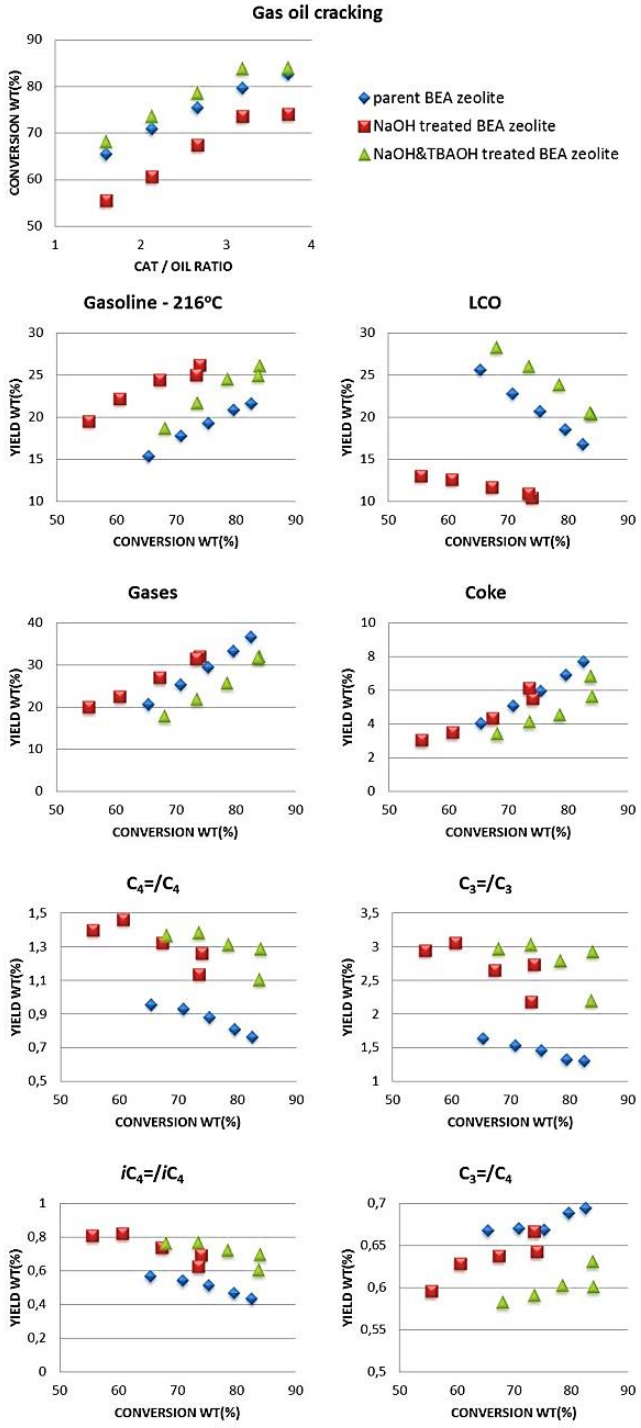
Gas oil cracking
CONVERSION WT(%)
CAT / OIL RATIO
parent BEA zeolite
NaOH treated BEA zeolite
NaOH&TBAOH treated BEA zeolite
Gasoline - 216°C
LCO
Gases
Coke
$C_4=/C_4$
$C_3=/C_3$
$iC_4=/iC_4$
$C_3=/C_4$
YIELD WT(%)
CONVERSION WT(%)

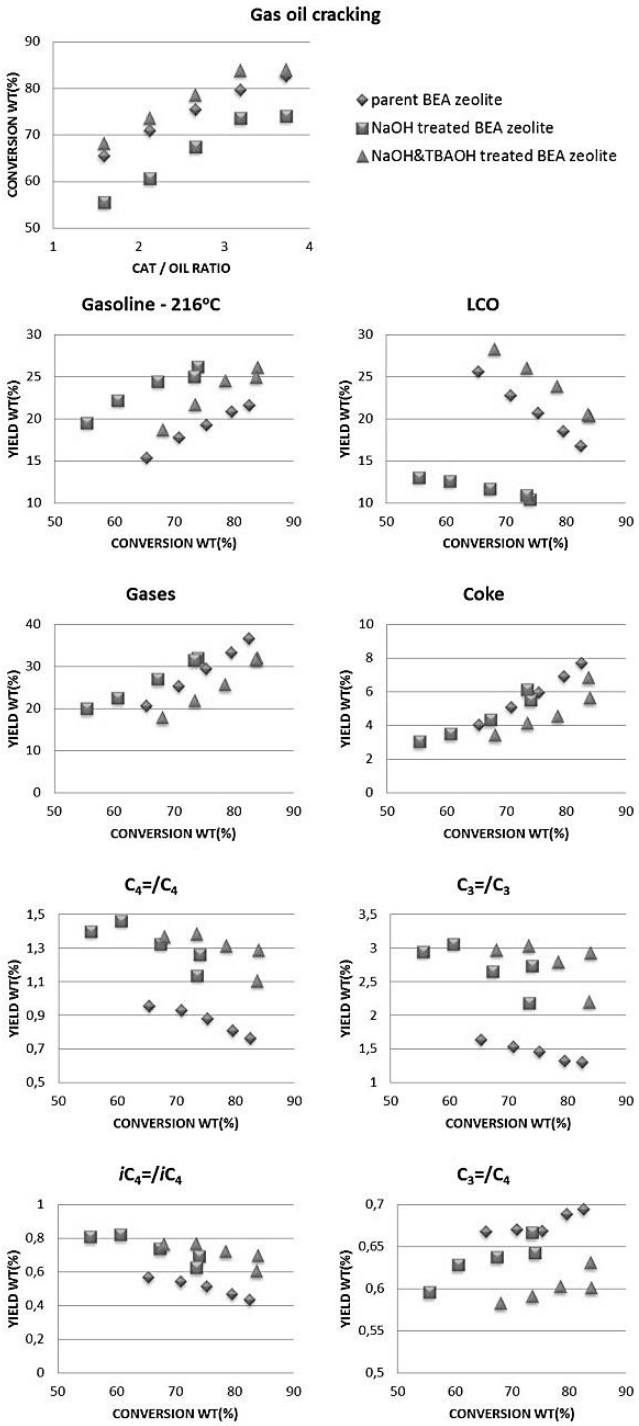
Gas oil cracking
CONVERSION WT(%)
CAT / OIL RATIO
parent BEA zeolite
NaOH treated BEA zeolite
NaOH&TBAOH treated BEA zeolite
Gasoline - 216ºC
LCO
Gases
Coke
$C_4=/C_4$
$C_3=/C_3$
$iC_4=/iC_4$
$C_3=/C_4$
YIELD WT(%)
CONVERSION WT(%)